Proceedings of the ASME Smart Materials, Adaptive Structures and Intelligent Systems
SMASIS2014
Sept. 8-10, 2014, Newport, Rhode Island, USA

SMASIS2014- 7529

TRAVELLING WAVE PHENOMENON THROUGH PIEZOELECTRIC ACTUATION OF A FREE-FREE BEAM

V. V. N. Sriram Malladi[1]*, Dragan Avirovik[2], Shashank Priya[2], Pablo A Tarazaga[1]

[1] Vibration, Adaptive Structures, and Testing Laboratory,
[2]Center for Energy Harvesting Materials and Systems (CEHMS),
Bio-Inspired Materials and Devices Laboratory (BMDL)
Department of Mechanical Engineering, Virginia Tech, Blacksburg, VA, USA

ABSTRACT

A mechanical wave is generated as a result of an oscillating body interacting with the well-defined medium and it propagates through that medium transferring energy from one location to another. The ability to generate and control the motion of the mechanical waves through the finite medium opens up the opportunities for creating novel actuation mechanisms. The focus of this study is on understanding the traveling wave generation and propagation by establishing the relationships that illustrate the role of structural and electromechanical parameters. A brass beam with free-free boundary conditions was selected to be the medium through which the wave propagation occurs. Two piezoelectric elements were bonded on the opposite ends of the beam and were used to generate the controlled oscillations. Excitation of the piezoelectrics results in coupled system dynamics that can be translated into generation of the waves with desired characteristics. Theoretical analysis based on the distributed parameter model and experiments were conducted to provide the comprehensive understanding of the wave generation and propagation behavior.

Keywords: Traveling waves, distributed parameter, FEM, piezoelectric materials, waves

*Address all correspondences to this author.

INTRODUCTION

Controlled oscillation of objects creates mechanical waves that propagate from one point to another through the surrounding medium. This study illustrates a novel actuation mechanism for generation and control of the traveling wave through the solid. It is well-known that two travelling waves of same amplitude and frequency moving in opposite directions will result in a standing wave on collision. When a solid structure is oscillated, two waves with identical amplitudes and frequency are generated and propagated in opposite direction. Due to the high impedance change at the ends of the structure, the waves are reflected back resulting in the formation of the standing waves. However, if the initial waves were of different amplitudes than the overall response would be a composite wave consisting of a traveling wave and a standing wave. A similar phenomenon is observed when a beam is actuated with two sinusoidal forces of identical frequencies [1]. The ratio between the traveling and standing wave in this case is observed to be dependent on many factors that includes phase difference, force amplitude, forcing frequency, location of forces, boundary conditions etc. Other methods for generating the traveling waves through solid structures can be achieved by adjusting the mechanical impedance using vibrators and absorbers [2], and/or using active control laws [3].

The study reported here is based on the primer method [1], where a beam is actuated by two forces at the same

frequency, but with phase difference. In order to fully understand the effect of the parameters (mainly frequency and phase) which contribute towards the wave propagation through solids, theoretical framework was established and presented in this work. Theoretical models for prediction and simulation of the dynamical response of free-free beam are presented. These models provide guidelines for actuation in order to accomplish the generation of traveling waves. Previously modeling and characterization of mechanical waves through finite medium has been has been conducted by Bucher et al. [4, 5]. Force excitation by vibration shakers at two different points at the same frequency but with phase difference of 90° was demonstrated to result in wave propagation.

In this study we have adopted the piezoelectric excitation for generation of the traveling wave through the brass beam. Detailed theoretical as well as experimental analysis was conducted in order to understand the dynamics of the free-free beam. Theoretical analysis based upon the distribution parameter model and experimental characterization was designed in such a way as to bring out the relevant physics of the traveling wave generation and propagation. Piezoelectric actuation allows for compact, miniature and cost-effective implementation of the concept on a variety of the intended platforms. We believe that this study will provide the basis required for understanding the fundamentals as the model can be easily extended towards maturing variety of applications.

THEORETICAL MODELING OF A PZT BEAM

Piezoelectric ceramic plates were used to excite a free-free brass beam. The theoretical basis of the analytical model was derived by calculating the net forces and moments generated by the piezoelectric plates on the same side of the beam. The electromechanical model takes into account the shift in the neutral axis due to these piezoelectric elements and uses voltage as a forcing function. A schematic diagram of the beam with the PZT patches is presented in Figure 1. The nomenclature used throughout this paper to describe the relative lengths and positions of the elements present in the beam is displayed in this figure. The beam is modeled as five distinct beam parts and each part is referred as a beam element throughout the paper. Three parts of the beam are substrate elements while the other two parts are composites of substrate and PZT patches.

The first step in modeling this complex system is to determine the shift of the neutral axis due to the presence of PZT plates on one side of the beam. The cross-sectional view of the beam depicting the shift of the neutral axis by a distance z_n is shown in Figure 2.

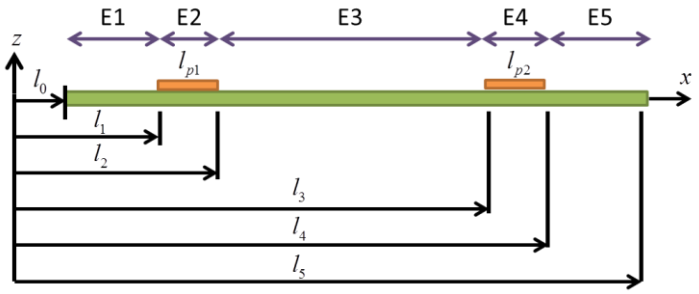

Figure 1. Free-Free beam with PZT patches and corresponding beam elements (E1-E5)

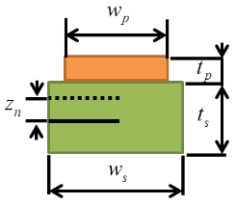

Figure 2. Cross-sectional view of the Free-Free beam with PZT patches

The new neutral axis is calculated by setting the sum of all the forces in the 1-direction (or along x-axis) over the entire cross-section to be zero:

$$\int_{-t_s/2}^{t_s/2} w_s \sigma_{s11} dz + \int_{t_s/2}^{t_s/2+t_p} w_p \sigma_{p11} dz = 0 \tag{1}$$

where the normal stresses of the substrate (σ_{s11}) and the piezo-ceramic (σ_{p11}) are expressed as a function of the beam displacement (w) using the well-known elastic strain-displacement relationships and the piezoelectric equations:

$$\begin{aligned} \sigma_{11s} &= Y_{1s} \cdot S_{11s} \\ &= -Y_{1s}(z - z_n)\frac{\partial^2 w(x,t)}{\partial x^2} \\ \sigma_{11p} &= Y_{1s} \cdot S_{11s} - Y_{1p} d_{13} E_3 \\ &= -Y_{1p}(z - z_n)\frac{\partial^2 w(x,t)}{\partial x^2} - Y_{1p} d_{13} E_3 \end{aligned} \tag{2}$$

The shift in the neutral axis is calculated in the no-excitation case i.e. when the electric field $E_3 = 0$. Upon simplification, we get the new location of the neutral axis at z_n as:

$$z_n = \frac{Y_{1p} w_p t_p (t_p + t_s)}{2(Y_{1s} w_s t_s + Y_{1p} w_p t_p)} \tag{3}$$

Euler Bernoulli beam equations were used to develop the electro-mechanical model of the free-free beam. The position of the piezo-ceramic elements on the beam is represented in the equation with the help of two terms: Heaviside function $\mathcal{H}(x)$ and identifier function $\chi_p(x)$. These terms have been used interchangeably depending on the situation. These terms are related by:

$$\chi_p(x) = \left[\mathcal{H}(x-l_2) - \mathcal{H}(x-l_1)\right] + \left[\mathcal{H}(x-l_4) - \mathcal{H}(x-l_3)\right] \tag{4}$$

Using the nomenclature defined previously, the net sum of the forces acting on the composite beam is determined to be:

$$\frac{\partial S}{\partial x} = \underbrace{\rho_s A_s \frac{\partial^2 w(x,t)}{\partial t^2}}_{Substrate} + \underbrace{\rho_p A_p \left[\mathcal{H}(x-l_2) - \mathcal{H}(x-l_1)\right] \frac{\partial^2 w(x,t)}{\partial t^2}}_{Left \quad Piezoceramic} + \underbrace{\rho_p A_p \left[\mathcal{H}(x-l_4) - \mathcal{H}(x-l_3)\right] \frac{\partial^2 w(x,t)}{\partial t^2}}_{Right \quad Piezoceramic} \tag{5}$$

where S(x) is the shear force acting on the beam element and the density and area of substrate and the pzt element are denoted by subscripts *"s"* and *"p"* respectively. Next the moments acting on the beam element were summed and this results in a relationship between the shear force and the bending moment given as:

$$S(x) = -\frac{\partial M(x)}{\partial x} \tag{6}$$

Substitution of this expression into (5) and simplifying, results in the relationship:

$$-\frac{\partial^2 M}{\partial x^2} = \left[\rho_s A_s + \rho_p A_p \cdot \chi_p(x)\right] \frac{\partial^2 w(x,t)}{\partial t^2} \tag{7}$$

The stress developed in this composite beam element is resultant of both mechanical properties of the composite beam and the electrical properties of the piezo-ceramic material. The stress can be expressed as:

$$\sigma_{11} = \underbrace{-(z-z_n)\frac{\partial^2 w(x,t)}{\partial x^2}\left\{Y_{1s} + Y_{1p} \cdot \chi_p(x)\right\}}_{Mechanical} \underbrace{- Y_{1p} d_{13} E_3 \cdot \chi_p(x)}_{Electrical} \tag{8}$$

This relationship between the stress induced in the beam and the deflection of the beam was used to determine the mechanical and electrical components of the moments generated in the beam element.

$$\begin{aligned} M &= M_{mech.} + M_{elec.} \\ &= \left[Y_s I_s + (Y_{sp} I_{sp} - Y_s I_s) \cdot \chi_p(x)\right] \frac{\partial^2 w(x,t)}{\partial x^2} \\ &\quad + \frac{Y_{1p} d_{13}}{t_p} Q V(x,t) \cdot \chi_p(x) \end{aligned}$$

where

$$\begin{aligned} Y_s I_s &= \frac{Y_{1s} w_s t_s^3}{12} \\ Y_{sp} I_{sp} &= \frac{Y_{1s} w_s}{3}\left[\left(\frac{t_s}{2} - z_n\right)^3 + \left(\frac{t_s}{2} + z_n\right)^3\right] \\ &\quad + \frac{Y_{1p} w_p}{3}\left[\left(\frac{t_s}{2} + t_p - z_n\right)^3 + \left(\frac{t_s}{2} + t_p + z_n\right)^3\right] \\ Q &= \frac{t_p}{2}(t_s + t_p) \quad and \quad E = \frac{V(x,t)}{t_p} \end{aligned} \tag{9}$$

When equation (9) is substituted into equation (7), a partial differential equation (PDE) that summarizes the electromechanical model of the composite beam is obtained:

$$\begin{aligned} &\left[\rho_s A_s + \rho_p A_p \cdot \chi_p(x)\right] \frac{\partial^2 w(x,t)}{\partial t^2} \\ &+ \frac{\partial^2}{\partial x^2}\left\{\left[Y_s I_s + (Y_{sp} I_{sp} - Y_s I_s) \cdot \chi_p(x)\right] \frac{\partial^2 w(x,t)}{\partial x^2}\right\} \\ &= -\frac{Y_{1p} d_{13}}{t_p} Q \cdot \frac{\partial^2}{\partial x^2}\left(V(x,t)\chi_p(x)\right) \end{aligned} \tag{10}$$

This model is used as an actuation guideline for traveling wave generation and it is validated through the experimental results.

DISTRIBUTED PARAMETER APPROACH

In the distributed parameter approach, separation-of-variables solution of the form $w(x,t) = X(x)T(t)$ is assumed. This solution is substituted into the equation of motion, equation (10), to yield:

$$-\frac{\ddot{T}(t)}{T(t)} = \frac{\frac{\partial^2}{\partial x^2}\left[B(x)X''(x)\right]}{A(x)X(x)} = \omega^2 \tag{11}$$

where

$$A(x)=\begin{cases}\rho_s A_s & \chi_p=0\\ \rho_s A_s+\rho_p A_p & \chi_p=1\end{cases} \quad (12)$$

and

$$B(x)=\begin{cases}Y_s I_s & \chi_p=0\\ Y_{sp} I_{sp} & \chi_p=1\end{cases} \quad (13)$$

The spatial equation comes from rearrangement of the equation(11), which results in:

$$\frac{\partial^2}{\partial x^2}\left[B(x)X''(x)\right]-\omega^2 A(x)X(x)=0 \quad (14)$$

The beam was modeled as five distinct beam parts, where the relationship between the parts was obtained through the displacement, slope, moment and shear force at their respective boundaries. The solution of the PDE for each of the five beam elements was assumed to be of the form

$$\begin{aligned}\Phi_n(x)&=A_n Sin\beta_n x+B_n Cos\beta_n x\\ &\quad +C_n Sinh\beta_n x+D_n Cosh\beta_n x\\ n&\in\{1,2,3,4,5\}\end{aligned} \quad (15)$$

where

$$\beta^4(x)=\frac{A(x)\omega^2}{B(x)} \quad (16)$$

The bending moment and shear force vanish at the free end of the beam. The continuity at the boundary between the substrate element and the composite element was achieved by equating displacement, slope, bending moment and shear forces at l_1, l_2, l_3 and l_4.

Boundary at l_0

$$\begin{aligned}&\phi_1''(x=0)=0\\ &\phi_1'''(x=0)=0\end{aligned} \quad (17)$$

Boundary at l_1

$$\begin{aligned}&\phi_1(x=l_1)=\phi_2(x=l_1)\\ &\phi_1'(x=l_1)=\phi_2'(x=l_1)\\ &Y_{1s}I_s\phi_1''(x=l_1)=Y_{sp}I_{sp}\phi_2''(x=l_1)\\ &Y_{1s}I_s\phi_1'''(x=l_1)=Y_{sp}I_{sp}\phi_2'''(x=l_1)\end{aligned} \quad (18)$$

Boundary at l_2

$$\begin{aligned}&\phi_2(x=l_2)=\phi_3(x=l_2)\\ &\phi_2'(x=l_2)=\phi_3'(x=l_2)\\ &Y_{sp}I_{sp}\phi_2''(x=l_2)=Y_{1s}I_s\phi_3''(x=l_2)\\ &Y_{sp}I_{sp}\phi_2'''(x=l_2)=Y_{1s}I_s\phi_3'''(x=l_2)\end{aligned} \quad (19)$$

Boundary at l_3

$$\begin{aligned}&\phi_3(x=l_3)=\phi_4(x=l_3)\\ &\phi_3'(x=l_3)=\phi_4'(x=l_3)\\ &Y_{1s}I_s\phi_3''(x=l_3)=Y_{sp}I_{sp}\phi_4''(x=l_3)\\ &Y_{1s}I_s\phi_3'''(x=l_3)=Y_{sp}I_{sp}\phi_4'''(x=l_3)\end{aligned} \quad (20)$$

Boundary at l_4

$$\begin{aligned}&\phi_4(x=l_4)=\phi_5(x=l_4)\\ &\phi_4'(x=l_4)=\phi_5'(x=l_4)\\ &Y_{sp}I_{sp}\phi_4''(x=l_4)=Y_{1s}I_s\phi_5''(x=l_4)\\ &Y_{sp}I_{sp}\phi_4'''(x=l_4)=Y_{1s}I_s\phi_5'''(x=l_4)\end{aligned} \quad (21)$$

Boundary at l_5

$$\begin{aligned}&\phi_5''(x=l_5)=0\\ &\phi_5'''(x=l_5)=0\end{aligned} \quad (22)$$

The 20 boundary conditions previously derived yield 20 equations in 20 unknown constants of integration which can be written as a matrix equation:

$$\begin{pmatrix}C_{1,1} & \cdots & \cdots & C_{1,20}\\ \vdots & \ddots & & \vdots\\ \vdots & & C'_{19\times19} & \vdots\\ C_{20,1} & \cdots & \cdots & C_{20,20}\end{pmatrix}_{20\times20}\begin{pmatrix}A_1\\ \vdots\\ A_{19}\\ A_{20}\end{pmatrix}_{20\times1}=\{0\}_{20\times1} \quad (23)$$

The matrix equation (23) will have a nonzero solution for the constants of integration, only if the determinant of the matrix **C** is singular. The elements of this equation are only a function of one variable, ω the natural frequency, as the other variables are either material constants or geometrical constants. By setting the determinant of the matrix **C** as zero, the natural frequencies were obtained.

$$\Delta[C]_{20\times20}=\begin{vmatrix}C_{1,1} & \cdots & \\ \vdots & \ddots & \vdots\\ & \cdots & C_{20,20}\end{vmatrix}=0 \quad (24)$$

Numerically the value of the determinant is computed at different values of ω and the frequency at which the determinant approaches zero was noted. This value of the determinant is plotted as a function of frequency in Figure 3.

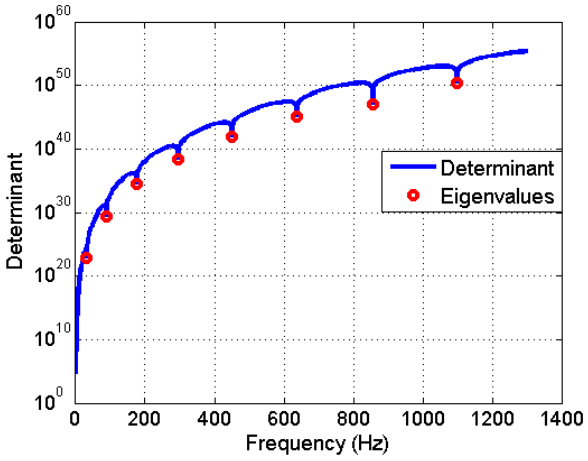

Figure 3 Determinant of the characteristic equation

The next step was determining the eigenvectors corresponding to these eigenvalues. There can be infinite solutions for the coefficients A_i, however a unique solution is obtained by setting one of the coefficients to 1. In this analysis A_1 is set to 1 and the remaining coefficients can be calculated numerically as:

$$\begin{pmatrix} C_{1,1} & \cdots & \cdots & C_{1,20} \\ \vdots & \boxed{C_{2,2}} & \cdots & \boxed{C_{2,20}} \\ \vdots & \vdots & C'_{19\times19} & \vdots \\ C_{20,1} & \underline{C_{20,2}} & \cdots & \underline{C_{20,20}} \end{pmatrix}_{20\times20} \begin{pmatrix} A_1 \\ \vdots \\ A_{19} \\ A_{20} \end{pmatrix}_{20\times1} = \{0\}_{20\times1} \quad (25)$$

where

$$[C']_{19\times19} \begin{bmatrix} A_2 \\ \vdots \\ \vdots \\ A_{20} \end{bmatrix}_{19\times1} + A_1 \begin{bmatrix} C_{2,1} \\ \vdots \\ \vdots \\ C_{20,1} \end{bmatrix}_{19\times1} = \{0\}_{19\times1} \quad (26)$$

This results in

$$\begin{bmatrix} A_2 \\ \vdots \\ \vdots \\ A_{20} \end{bmatrix}_{19\times1} = -[C']^{-1}_{19\times19} \cdot A_1 \begin{bmatrix} C_{2,1} \\ \vdots \\ \vdots \\ C_{20,1} \end{bmatrix}_{19\times1} \quad (27)$$

In-order to normalize the mode shapes obtained from the coefficients derived in the previous step, a mass term (N_{mass}) is calculated by using the principle of orthogonality of the mode shapes throughout the length of the beam.

$$\begin{aligned} N_{mass} &= \rho_s A_s \int_{l_0}^{l_1} \Phi_1{}^2(x)dx \\ &+(\rho_s A_s + \rho_p A_p)\int_{l_1}^{l_2} \Phi_2{}^2(x)dx \\ &+\rho_s A_s \int_{l_2}^{l_3} \Phi_3{}^2(x)dx \\ &+(\rho_s A_s + \rho_p A_p)\int_{l_3}^{l_4} \Phi_4{}^2(x)dx \\ &+\rho_s A_s \int_{l_4}^{l_5} \Phi_5{}^2(x)dx \end{aligned} \quad (28)$$

The normalized mode shape is the spatial solution of the composite beam and it is defined as ($\tilde{\Phi}_i$): :

$$\tilde{\Phi}_i = \frac{\Phi_i}{\sqrt{N_{mass}}} \qquad i = 1,..,5 \quad (29)$$

The next modeling step is to find the solution of the temporal part of the composite equation. It can be seen from equation (10) that the forcing term is presented as the voltage applied to the piezoelectric material. This shows that the temporal solution needs to be derived for those beam elements which include the piezo properties.

$$l_0 \le x < l_1$$
$$\rho_s A_s \frac{\partial^2 w(x,t)}{\partial t^2} + \frac{\partial^2}{\partial x^2}\left\{ Y_s I_s \frac{\partial^2 w(x,t)}{\partial x^2} \right\} = 0 \quad (30)$$

$$l_1 \le x < l_2$$
$$(\rho_s A_s + \rho_p A_p)\frac{\partial^2 w(x,t)}{\partial t^2} + \frac{\partial^2}{\partial x^2}\left\{ Y_{sp} I_{sp} \frac{\partial^2 w(x,t)}{\partial x^2} \right\} = -\frac{Y_{1p} d_{13}}{t_p} Q \cdot \frac{\partial^2}{\partial x^2}\left(V(x,t)\chi_p(x) \right)$$

$$l_2 \le x < l_3$$
$$\rho_s A_s \frac{\partial^2 w(x,t)}{\partial t^2} + \frac{\partial^2}{\partial x^2}\left\{ Y_s I_s \frac{\partial^2 w(x,t)}{\partial x^2} \right\} = 0 \quad (31)$$

$$l_3 \le x < l_4$$
$$(\rho_s A_s + \rho_p A_p)\frac{\partial^2 w(x,t)}{\partial t^2} + \frac{\partial^2}{\partial x^2}\left\{ Y_{sp} I_{sp} \frac{\partial^2 w(x,t)}{\partial x^2} \right\} = -\frac{Y_{1p} d_{13}}{t_p} Q \cdot \frac{\partial^2}{\partial x^2}\left(V(x,t)\chi_p(x) \right) \quad (32)$$

$$l_4 \le x \le l_5$$
$$\rho_s A_s \frac{\partial^2 w(x,t)}{\partial t^2} + \frac{\partial^2}{\partial x^2}\left\{ Y_s I_s \frac{\partial^2 w(x,t)}{\partial x^2} \right\} = 0 \tag{33}$$

The particular solution is available for the portions of the beam that lie in the regions $[l_1 \quad l_2]$ and $[l_3 \quad l_4]$. Multiplying equation (10) by $\tilde{\Phi}_i$ and integrating over the length of the beam yields:

$$\begin{bmatrix} \rho_s A_s \int_{l_0}^{l_1} \tilde{\Phi}_1(x)\cdot\tilde{\Phi}_1(x)dx \\ +\rho_{sp} A_{sp} \int_{l_1}^{l_2} \tilde{\Phi}_2(x)\cdot\tilde{\Phi}_2(x)dx \\ +\rho_s A_s \int_{l_2}^{l_3} \tilde{\Phi}_3(x)\cdot\tilde{\Phi}_3(x)dx \\ +\rho_{sp} A_{sp} \int_{l_3}^{l_4} \tilde{\Phi}_4(x)\cdot\tilde{\Phi}_4(x)dx \\ +\rho_s A_s \int_{l_4}^{l_5} \tilde{\Phi}_5(x)\cdot\tilde{\Phi}_5(x)dx \end{bmatrix} \times \left(\ddot{T}(t) + \omega^2 T(t)\right)$$
$$= -\frac{Y_{1p} d_{13}}{t_p} Q \left[\int_{l_0}^{l_5} \frac{\partial^2}{\partial x^2}\left(V(x,t)\chi_p(x)\right)\cdot\tilde{\Phi}(x)dx \right] \tag{34}$$

Upon simplifying with the help of the othogonality principle and the Dirac delta identities, this equation is reduced to:

$$-\frac{Y_{1p} d_{13}}{t_p} Q \begin{bmatrix} Ve^{j\omega t}\left(\tilde{\Phi}'_3(l_2) - \tilde{\Phi}'_2(l_1)\right) \\ +Ve^{j(\omega t+\phi)}\left(\tilde{\Phi}'_5(l_4) - \tilde{\Phi}'_4(l_3)\right) \end{bmatrix} = \left(\ddot{T}(t) + \omega_n{}^2 T(t)\right) \tag{35}$$

The damping term is then introduced into this equation and this yields:

$$\left(\ddot{T}(t) + 2\zeta\omega_n \dot{T}(t) + \omega_n{}^2 T(t)\right)$$
$$= -\frac{Y_{1p} d_{13}}{t_p} Q \begin{bmatrix} Ve^{j\omega t}\left(\tilde{\Phi}'_3(l_2) - \tilde{\Phi}'_2(l_1)\right) \\ +Ve^{j(\omega t+\phi)}\left(\tilde{\Phi}'_5(l_4) - \tilde{\Phi}'_4(l_3)\right) \end{bmatrix} \tag{36}$$

Finally the frequency response function (FRF) for a single piezo-ceramic was derived as shown below:

$$T(\omega) = \frac{-Y_{1p} d_{13} Q\left(\tilde{\Phi}'_3(l_2) - \tilde{\Phi}'_2(l_1)\right)}{t_p(\omega_n{}^2 - \omega^2 + 2j\zeta\omega)} \cdot V(\omega) \tag{37}$$

First, the response of each individual piezo is numerically computed and then the overall response is obtained by the principle of superposition. The eigenvalues and eigenvectors of this theoretical model are first validated against the experimental results and finite element model for a free-free beam and then traveling wave behavior is discussed.

EXPERIMENTAL SETUP AND TEST PROCEDURE

An experimental characterization in the lab was performed in order verify the theoretical model discussed in the previous section, Figure 4. A brass beam with length=0.305m, width=0.0195m and thickness=0.000832m was suspended on elastic bands in order to simulate free-free boundary conditions. The physical properties of the composite beam are provided in Table 1.

Table 1 Physical properties of the composite beam

Parameter	Data
Length of beam	0.305 *m*
Material of substrate	Brass
Young's Modulus of substrate	100 *GPa*
Density of substrate	8430 kg/m^3
Thickness of substrate	0.832 *mm*
Width of substrate	19.5 *mm*
Type of PZT	PZT-5A
Density of PZT	7800 kg/m^3
Young's Modulus of PZT	62 *GPa*
Thickness of PZT	0.191 *mm*

Figure 4 Experimental setup to study the traveling waves generated on a free-free beam

The response of the vibrating system was experimentally measured using a Laser Scanning Vibrometer and data acquisition system (PSV400, Polytec Inc.) as shown in Figure 4. With the help of this experimental setup, a model test was carried out to detect the resonance frequencies and the

corresponding mode shape. In these modal tests, a single piezoelectric plate is excited and the response is measured by the vibrometer. The frequency response function of the beam is shown in Figure 5

.

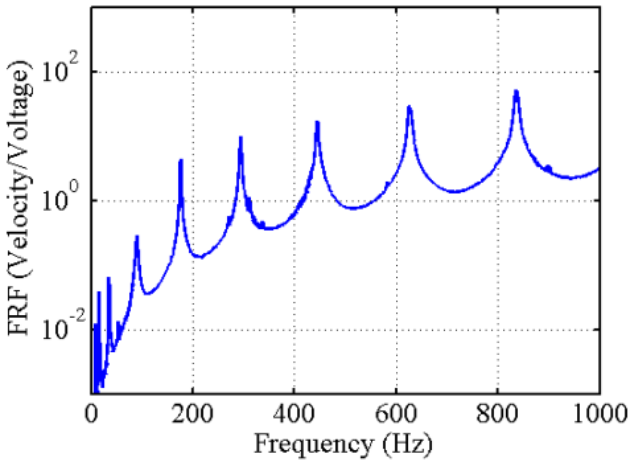

Figure 5 Experimentally obtained frequency response function (FRF) of a free-free beam

Travelling waves are generated by exciting the two piezo-ceramics at the same frequency but with a phase difference of 90º. A comparison between the results obtained experimentally and those obtained theoretically are presented in the section that follows.

Table 2 Comparison of the experimental, theoretical and FEM model predicted resonant frequencies of a free-free beam

Frequency order	Exp. (Hz)	DP. (Hz)	Error %	FEM (Hz)	Error %
1	35.00	31.27	10.65	32.5	7.142
2	89.69	87.78	2.129	87.94	1.951
3	175.9	175.0	0.511	175.9	0
4	293.4	295.0	0.545	296.3	0.988
5	444.4	449.2	1.080	451.2	1.530
6	625.3	637.4	1.935	642.4	2.734
7	835.3	856.5	2.538	862.2	3.220

RESULTS AND DISCUSSION

Validation of the theoretical model was conducted by comparing the eigenvalues and eigenvectors against the experimental results and finite element model (FEM) results. The response of the vibrating system was experimentally measured using a Laser Scanning Vibrometer and data acquisition system (PSV400, Polytec Inc.). The results are tabulated in Table 2. These results show that most of the eigenvalues predicted by the models match with the experimental values with an error less than 3%. The mode shapes of the first five resonant frequencies as predicted by the distributed parameter model are presented in Figure 6.

In-order to generate the traveling waves, two sinusoidal voltage signals of equal magnitudes but separated by a phase difference of 90º were applied onto the two piezoelectric ceramic plates. The frequency of excitation was chosen to lie half-way between any two eigenvalues representing the bending modes of the system.

A clear distinction between the traveling waves and standing waves can be identified from Figure 7. As presented, the standing wave behavior is identified by the presence of nodal points in Figure 7a. In the case of a traveling wave, as the wave is swept from one end of the beam to the other, a continuous and uniform area is seen (absence of nodal points) in Figure 7b. The limits or the envelope representing the wave profile is sufficient to determine the quality of the wave.

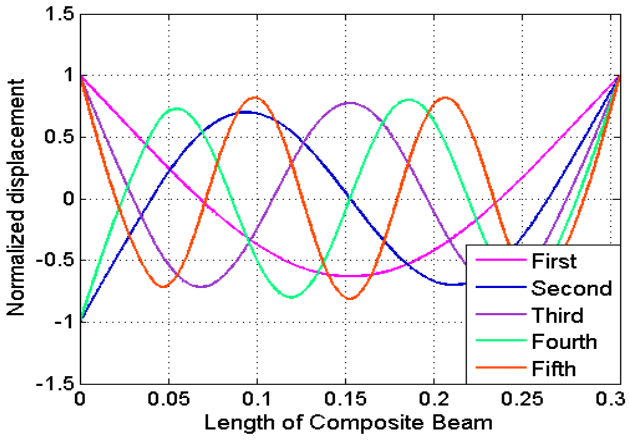

Figure 6 Mode shapes of the composite beam using distributed parameter model

Finally, a comparison between the results obtained theoretically and experimentally is presented in Figure 8. Figure 8a compares the traveling wave behavior when the beam is excited at 133Hz (a frequency between the second and third natural frequency) while Figure 8b studies the frequency between the third and fourth resonant frequency (241Hz). These results demonstrate that both the FEM and distributed parameter model capture the experimental results very well.

CONCLUSIONS

In conclusion, this study provides the model for the composite beam with a brass substrate and two piezoelectric plates attached near the two ends. Detailed description of the distributed parameter model was presented. Validation of the distributed parameter model was achieved by comparing it

with the experimental data and FEM model. The results showed that the theoretical model was able to predict the dynamics of the traveling waves quite accurately. It is believed that this study will provide significant assistance in the development of traveling wave inspired propulsion devices and micro-organisms.

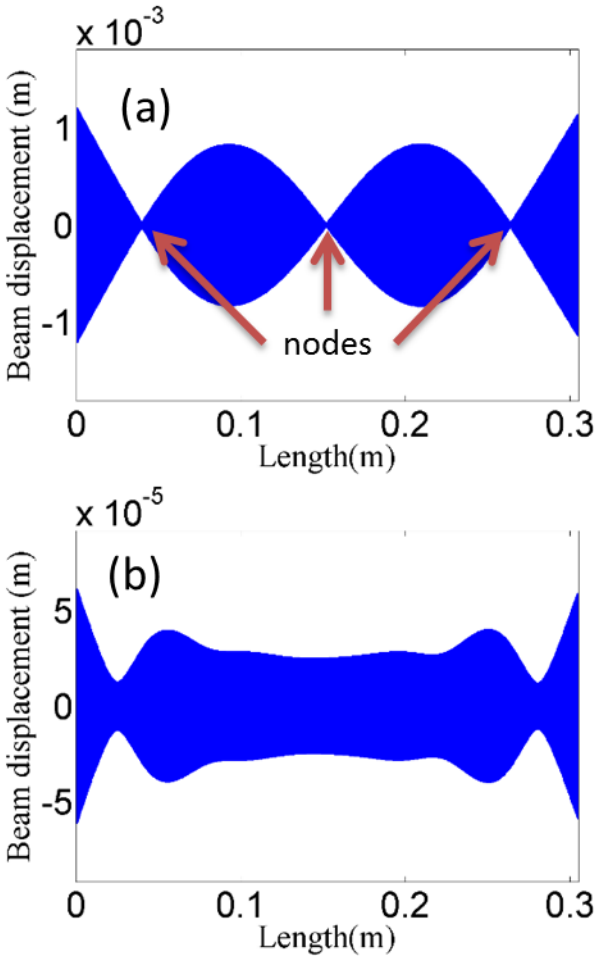

Figure 7 Area swept by a standing wave (top figure) and a travelling wave (bottom figure)

ACKNOWLEDGEMENT

The authors (D.A. and S. P.) gratefully acknowledge the financial support from NSF INAMM program.

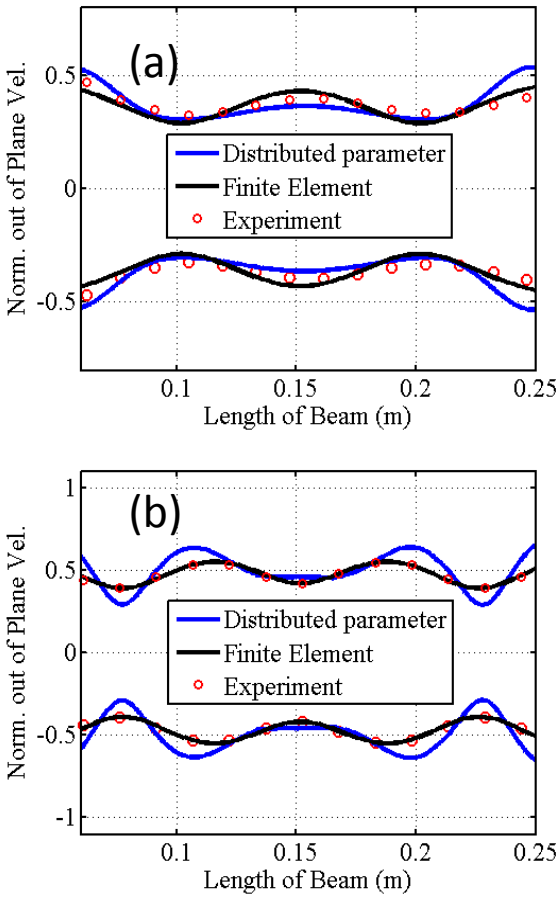

Figure 8 Traveling wave envelope obtained experimentally and theoretically. Actuation was conducted at a frequency between two mode shapes with phase difference of 90° a)133Hz b) 241Hz

REFERENCES

[1] Loh, B.-G., Ro, P. I., "An object transport system using flexural ultrasonic progressive waves generated by two-mode excitation," Ultrasonics, Ferroelectrics and Frequency Control, IEEE Transactions on, 47, 994-999, (2000).

[2] Kuribayashi, M., Ueha, S., Mori, E., "Excitation conditions of flexural traveling waves for a reversible ultrasonic linear motor," The Journal of the Acoustical Society of America, 77, 1431-1435, (1985).

[3] Hashimoto, Y., Koike, Y., Ueha, S., "Near-field acoustic levitation of planar specimens using flexural vibration," The Journal of the Acoustical Society of America, 100, 2057-2061, (1996).

[4] Bucher, I., "Estimating the ratio between travelling and standing vibration waves under non-stationary conditions," Journal of sound and vibration, 270, 341-359, (2004).

[5] Minikes, A., Gabay, R., Bucher, I., et al., "On the sensing and tuning of progressive structural vibration waves," Ultrasonics, Ferroelectrics and Frequency Control, IEEE Transactions on, 52, 1565-1576, (2005).